DALTON

Synthesis of the 17-electron cations $[FeL(L')(NO)_2]^+$ (L, L' = PPh_3, $OPPh_3$): structure and bonding in four-co-ordinate metal dinitrosyls, and implications for the identity of paramagnetic iron dinitrosyl complex catalysts*

Francis L. Atkinson,[a] Helen E. Blackwell,[a] Nathan C. Brown,[a] Neil G. Connelly,[a] John G. Crossley,[a] A. Guy Orpen,[a] Anne L. Rieger[b] and Philip H. Rieger[b]

[a] *School of Chemistry, University of Bristol, Bristol BS8 1TS, UK*
[b] *Department of Chemistry, Brown University, Providence, RI 02912, USA*

The complex $[FeL_2(NO)_2]$ (L = PEt_3 **1a**, L = PPh_3 **1b** or L_2 = dppe **1c**) prepared from $[\{Fe(\mu\text{-}I)(NO)_2\}_2]$ and PPh_3 or $Ph_2PCH_2CH_2PPh_2$ (dppe) {in the presence and absence of $[Co(cp)_2]$ (cp = η^5-C_5H_5) respectively} undergo one-electron oxidation at a platinum electrode in CH_2Cl_2. The complex $[\{Fe(\mu\text{-dppm})(NO)_2\}_2]$ **2**, prepared from $[\{Fe(\mu\text{-}I)(NO)_2\}_2]$ and $Ph_2PCH_2PPh_2$ (dppm) in the presence of $[Co(cp)_2]$, undergoes two sequential one-electron oxidations. Complex **1b** with $[Fe(cp)_2]^+$ gave $\mathbf{1b}^+$, X-ray studies of which show a distorted tetrahedral geometry with near C_{2v} symmetry. Oxidation of **1b** leads to substantial lengthening of the Fe–P bonds and changes in the P–Fe–P and N–Fe–N angles. These changes are consistent with significant Fe–P π-bonding character in the singly occupied molecular orbital of $\mathbf{1b}^+$. Cation $\mathbf{1b}^+$ reacts with halide ions, giving $[FeX(PPh_3)(NO)_2]$ (X = Cl or I) and then $[FeX_2(NO)_2]^-$, and with $OPPh_3$ to give $[Fe(OPPh_3)(PPh_3)(NO)_2]^+$ $\mathbf{3}^+$. X-Ray studies on the last, as its $[PF_6]^-$ salt, show a distorted tetrahedral geometry; the co-ordination angles at iron approach trigonal bipyramidal with the PPh_3 ligand in one apical site and the other apical site vacant. The complex $[Fe(OPPh_3)_2(NO)_2]^+$ $\mathbf{4}^+$ resulted from the reaction between $[\{Fe(\mu\text{-}I)(NO)_2\}_2]$ and $OPPh_3$ in the presence of $TlPF_6$. An analysis of the ESR spectra of the paramagnetic cations $\mathbf{1b}^+$, $\mathbf{3}^+$ and $\mathbf{4}^+$, together with extended-Hückel MO calculations on models of $\mathbf{1b}^+$ and $\mathbf{3}^+$, suggest that the complex catalysts formed from $[\{Fe(\mu\text{-Cl})(NO)_2\}_2]$ and Ag^+ or Tl^+ are also four-co-ordinate 17-electron radicals. A crystallographic database study of four-co-ordinate dinitrosyl complexes of iron and other metals confirms that the N–Fe–N and O···Fe···O angles are linearly related. Consideration of these geometric effects, and those resulting from oxidation of **1b**, in the light of a model proposed by Summerville and Hoffmann provides insight into the bonding in these and related species.

Two series of four-co-ordinate iron dinitrosyl phosphine complexes exist,[1] namely 18-electron species with the general formula $[FeL_2(NO)_2]$ (L = phosphine or phosphite) and 17-electron radicals typified by $[FeXL(NO)_2]$ (X = halide). The former may be prepared[2,3] by reducing the latter in the presence of L. However, oxidation of the former to give $[FeL_2(NO)_2]^+$ has not been reported even though $[Fe(bipy)(NO)_2]^+$ (bipy = 2,2′-bipyridine)[4] and $[FeL^1{}_2(NO)_2]^+$ (L^1 = 1,3-dimethylimidazolidin-2-ylidene)[5] have been generated from $[Fe(bipy)(NO)_2]$ and $[FeL^1{}_2(NO)_2]$ and characterised by ESR spectroscopy.

We now describe electrochemical, synthetic and spectroscopic studies of the interconversion of $[FeXL(NO)_2]$ and $[FeL_2(NO)_2]$, thereby defining a redox-based square scheme in which the 17-electron species are activated towards substitution by one-electron reduction and the 18-electron complexes by one-electron oxidation. Moreover, X-ray structural studies on $[Fe(PPh_3)_2(NO)_2][PF_6]$ and $[Fe(OPPh_3)(PPh_3)(NO)_2][PF_6]$, extended-Hückel molecular orbital (EHMO) calculations, and ESR spectroscopic studies on the paramagnetic cations not only further define the geometric and electronic structures of four-co-ordinate complexes $[ML_2(NO)_2]$ but also show that the catalytically active species generated[6–8] by the reaction of $[\{Fe(\mu\text{-Cl})(NO)_2\}_2]$ with silver(I) or thallium(I) salts in tetrahydrofuran (thf), MeCN, *etc.*, most likely have tetrahedral (17-electron) structures.

Results and Discussion

Synthesis of 18-electron complexes

The complex $[FeL_2(NO)_2]$ **1a** (L = PEt_3) was prepared by the thermal reaction of $[Fe(CO)_2(NO)_2]$ with PEt_3 using a modification of the published procedure.[9] However, complexes **1** [L = PPh_3 **1b** or L_2 = dppe ($Ph_2PCH_2CH_2PPh_2$) **1c**] were prepared more efficiently by the one-electron reduction of $[FeXL(NO)_2]$, a route avoiding the use of the toxic liquid dicarbonyl.

The reaction of $[FeI(PPh_3)(NO)_2]$ with PPh_3, for which kinetic studies have been reported,[10] slowly (*ca.* 1 d) yields **1b** (L = PPh_3); an excess of PPh_3 is required to scavenge the displaced iodine. However, the reaction is considerably accelerated when carried out in the presence of a reductant. Previous syntheses have involved the use of sodium amalgam[2] or of zinc or copper powder[3] but **1b** is rapidly and more conveniently prepared by the addition of 1 equivalent of $[Co(cp)_2]$ (cp = η^5-C_5H_5) to an equimolar mixture of PPh_3 and $[FeI(PPh_3)(NO)_2]$ (prepared *in situ* from $[\{Fe(\mu\text{-}I)(NO)_2\}_2]$ and PPh_3) in toluene; after removing solid $[Co(cp)_2]I$ by filtration the product is precipitated with *n*-hexane. One-electron reduction of $[FeI(PPh_3)(NO)_2]$ to $[FeI(PPh_3)(NO)_2]^-$, followed by loss of iodide ion, accelerates PPh_3 co-ordination.

Complex **1c** was prepared by adapting the literature

* *Supplementary data available* (No. SUP 57156, 12 pp.): molecular orbital calculations. See instructions for Authors, *J. Chem. Soc., Dalton Trans.*, 1996, Issue 1.

Non-SI unit employed: G = 10^{-4} T.

Table 1 Analytical and IR spectroscopic data for the iron dinitrosyl complexes

Complex	Colour	Yield (%)	Analysis (%)[a] C	H	N	IR[b]/cm^{-1} ν(NO)
2 [{Fe(μ-dppm)(NO)$_2$}$_2$][c]	Ochre	54	60.5 (60.5)	5.0 (4.9)	5.0 (5.2)	1733, 1721 1687,[d] 1668
1b$^+$ [Fe(PPh$_3$)$_2$(NO)$_2$]$^+$ [e]	Black	66	54.8 (55.1)	3.7 (3.9)	3.5 (3.6)	1814, 1766
3$^+$ [Fe(OPPh$_3$)(PPh$_3$)(NO)$_2$]$^+$ [e]	Violet	51	54.1 (54.0)	3.8 (3.8)	3.2 (3.5)	1809, 1746
4$^+$ [Fe(OPPh$_3$)$_2$(NO)$_2$]$^+$ [e,f]	Beige	50	49.9 (49.3)	3.6 (3.6)	3.0 (3.0)	1813,[d] 1734
1a [Fe(PEt$_3$)$_2$(NO)$_2$]	—	—	—	—	—	1694, 1647
1b [Fe(PPh$_3$)$_2$(NO)$_2$]	—	—	—	—	—	1714, 1668
1c [Fe(dppe)(NO)$_2$]	—	—	—	—	—	1716, 1668

[a] Calculated values in parentheses. [b] In CH_2Cl_2; strong absorptions unless otherwise stated. [c] Analysed as a 1 : 1 thf solvate. [d] Medium absorption. [e] Isolated as PF_6^- salt. [f] Analysed as a 1 : 1 CH_2Cl_2 solvate.

method.[11] The addition of 2 equivalents of dppe to [{Fe(μ-I)(NO)$_2$}$_2$] in toluene gave a green-brown precipitate and a solution of **1c** almost immediately; the same reaction using [{Fe(μ-Cl)(NO)$_2$}$_2$] appears to be slower.[11] The reaction of [{Fe(μ-I)(NO)$_2$}$_2$] with dppe differs from that with PPh_3 in that it is rapid even in the absence of [Co(cp)$_2$]; it may occur *via* the direct substitution of iodine, or *via* disproportionation as proposed for the reaction of [{Fe(μ-Cl)(NO)$_2$}$_2$] with dppe.[12]

The reaction of [{Fe(μ-I)(NO)$_2$}$_2$] with dppm (Ph_2P-CH_2PPh_2) differs from that with dppe. The addition of 1 equivalent of dppm to 1 equivalent of the dimer in toluene gave a solution showing nitrosyl absorptions at 1798 and 1742 cm^{-1}. On adding a second equivalent of the phosphine an olive green solution is formed and new bands at 1793 and 1739 cm^{-1} are observed. The second pair of bands is almost identical in energy to that of [FeI(PPh$_3$)(NO)$_2$] suggesting, together with the stoichiometry of the reaction, the formation of [FeI(η^1-dppm)(NO)$_2$]. The first product is then most likely [{FeI(NO)$_2$}$_2$(μ-dppm)], an analogue of [{FeCl(NO)$_2$}$_2$(μ-dppe)] which has been prepared from [{Fe(μ-Cl)(NO)$_2$}$_2$] and 1 equivalent of dppe.[11] Whereas [{FeCl(NO)$_2$}$_2$(μ-dppe)] then reacts with an excess of dppe to give [Fe(dppe)(NO)$_2$], [{FeI(NO)$_2$}$_2$(μ-dppm)] and dppm give only [FeI(η^1-dppm)(NO)$_2$]; no evidence was found for iodine substitution.

The monodentate dppm complex [FeI(η^1-dppm)(NO)$_2$] does, however, react immediately with 1 equivalent of [Co(cp)$_2$] to give a yellow precipitate of [Co(cp)$_2$]I and a red-brown solution from which ochre microcrystals (**2**) were isolated. The elemental analysis (C, H and N) (Table 1) and ^{1}H NMR spectrum of complex **2** were in agreement with the formation of [Fe(dppm)(NO)$_2$]·0.5thf. However, the IR spectrum shows four nitrosyl stretching absorptions, consistent with a dimeric, dppm-bridged structure, *i.e.* with the formula [{Fe(μ-dppm)(NO)$_2$}$_2$]·thf; the dimers [{Fe(μ-dmpz)(NO)$_2$}$_2$] (dmpz = 3,5-dimethylpyrazolyl)[13] and [{Ni(CO)$_2$(μ-dppm)}$_2$][14] similarly show four absorptions (nitrosyl and carbonyl bands respectively).

Why the reactions of [{Fe(μ-I)(NO)$_2$}$_2$] with dppe and dppm are so different is unknown though the smaller bite angle of the latter may prevent the formation of the chelated monomer [Fe(dppm)(NO)$_2$]. Hence, there is no driving force for the elimination of iodine from [FeI(η^1-dppm)(NO)$_2$]. Once again, however, one-electron reduction, to [FeI(η^1-dppm)(NO)$_2$]$^-$, is followed by the facile loss of iodide ion, in this case giving the bridged dimer rather than the chelated monomer.

Electrochemical studies on complexes 1 and 2

Cyclic voltammetry at a platinum disc electrode shows that each of the three complexes **1a**–**1c** undergoes oxidation in CH_2Cl_2 at a potential in the range *ca.* 0.2–0.5 V; no further oxidation was observed to 1.80 V and no reduction waves were observed in the range 0.0 to −1.80 V. For **1b**, the oxidation wave ($E^{\circ\prime}$ = 0.37 V) is diffusion controlled and fully reversible, and is also so in MeCN ($E^{\circ\prime}$ = 0.36 V) suggesting that the monocation [FeL$_2$(NO)$_2$]$^+$ (**1b**$^+$) is stable on the cyclic voltammetric time-scale even in the co-ordinating nitrile solvent.

Complex **1a** is oxidised at 0.21 V; the less positive potential (*cf.* **1b**) is in accord with the presence of the stronger donor ligand which also results in lower energy IR nitrosyl absorptions (Table 1). By contrast, although the ν(NO) values for **1c** and **1b** are very similar (Table 1), the former complex is considerably more difficult to oxidise ($E^{\circ\prime}$ = 0.53 V) than the latter. Correlations between $E^{\circ\prime}$ and ν(CO)[15] or ν(NO)[16] have been observed previously. That such a relationship does not seem to hold for **1** may result from the different steric requirements of the monodentate phosphine (PPh_3 and PEt_3) and bidentate dppe ligands leading to a lower energy for the highest occupied molecular orbital (HOMO) of **1c** associated with the lower P–Fe–P angle in **1c** as compared with **1b** (85.9[11] *vs.* 112.3°[17]). Summerville and Hoffmann[18] have reported that HOMO energies in d^{10} MX_2Y_2 species isoelectronic with **1** are lowered on reduction of the X–Fe–X angles.

The cyclic voltammogram of the binuclear complex [{Fe(μ-dppm)(NO)$_2$}$_2$] **2** is very different from those of **1** in showing two oxidation waves in the range 0.0–1.8 V. The first ($E^{\circ\prime}$ = 0.40 V) is fully reversible but the second is only partially so (i_{red}/i_{ox} *ca.* 0.7; scan rate 200 mV s^{-1}) with the oxidation peak potential, $(E_p)_{ox}$, at 0.72 V and the associated reduction peak potential, $(E_p)_{red}$, at 0.59 V. The observation of two oxidation waves, rather than the single wave for **1**, is consistent with the proposed dimeric formulation. Moreover, the separation of the two waves by *ca.* 0.25 V suggests that one-electron oxidation may lead to a delocalised mixed-valence monocation [{Fe(μ-dppm)(NO)$_2$}$_2$]$^+$ (see below).

Synthesis of complex 1b$^+$

On the basis of the electrochemical studies noted above, the monocations **1**$^+$ were expected to be formed by treating **1** with mild one-electron oxidants. Accordingly, the addition of 1 equivalent of [Fe(cp)$_2$][PF$_6$] to **1b** in CH_2Cl_2 gave a dark brown solution from which brown crystals of [Fe(PPh$_3$)$_2$(NO)$_2$][PF$_6$] were obtained in good yield. The paramagnetic salt, which is stable when stored under nitrogen at −10 °C, was characterised by elemental analysis (Table 1), its cyclic voltammogram, which showed one reversible wave at a potential identical to that for the oxidation of **1b** (and confirmed as a reductive process by voltammetry at a rotating platinum electrode), and by IR and ESR spectroscopy (see below).

In CH_2Cl_2, the cation [Fe(PPh$_3$)$_2$(NO)$_2$]$^+$ **1b**$^+$ shows two

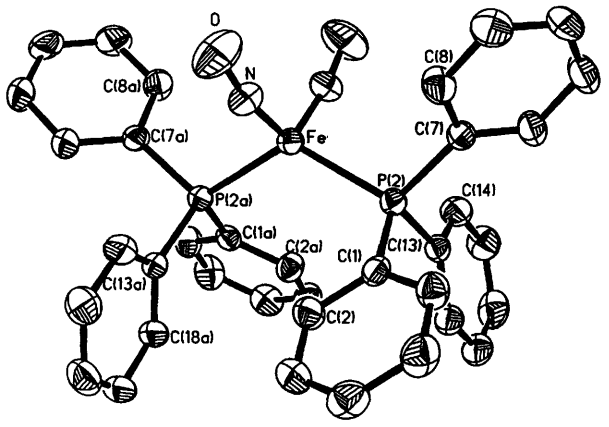

Fig. 1 Molecular structure of the cation of [**1b**]PF_6 showing the atom labelling scheme. All hydrogen atoms have been omitted for clarity

nitrosyl bands shifted to higher wavenumber (by *ca.* 100 cm^{-1}) from those of **1b**, a shift consistent with a metal-based oxidation. The relative intensities of the two nitrosyl absorptions are very similar to those of **1b** implying retention of the tetrahedral structure. Among the many known 17- and 18-electron four-co-ordinate iron dinitrosyls, **1b** and **1b**$^+$ constitute a unique, isolable redox pair. Accordingly, an X-ray structural study was carried out on crystals of $[Fe(PPh_3)_2(NO)_2][PF_6]$ in order to make a detailed comparison with the structure of **1b**.[17]

Crystal-structure determination of [1b]PF_6

Crystals suitable for X-ray diffraction studies were grown by allowing a concentrated solution of **1b**$^+$, as the $[PF_6]^-$ salt, in CH_2Cl_2 to diffuse into *n*-hexane at −10 °C. The molecular structure is shown in Fig. 1, and selected molecular geometry data are listed in Table 2. In the crystal structures of both **1b** and [**1b**]PF_6 the complex has exact (crystallographic) C_2 and approximate C_{2v} symmetry. The cation shows approximately tetrahedral co-ordination at iron and near linear nitrosyl ligands, as expected. The effects of oxidation on the structure **1b** are further discussed below.

Reactions of 1b$^+$

Unlike **1b**, cation **1b**$^+$ is substitutionally labile. Although stable for short periods in CH_2Cl_2 under an inert atmosphere it decomposes rapidly in more polar solvents such as thf or MeCN. During such decomposition, some **1b** is produced, possibly by a nucleophile-induced disproportionation reaction of the type observed when pyridine reacts with $[Fe(CO)_3(PPh_3)_2]^+$.[19]

The reaction of **1b**$^+$ with 1 equivalent of halide ion is better defined than that with polar solvents, giving the known[1] neutral complexes $[FeX(PPh_3)(NO)_2]$ (X = Cl or I). The displacement of PPh_3 from **1b**$^+$ by X^- thus completes a series of reactions in which the two types of four-co-ordinate iron dinitrosyl complex, $[FeL_2(NO)_2]$ and $[FeXL(NO)_2]$, are interconverted. This interconversion may be represented by a 'square scheme' (Scheme 1) in which one-electron oxidation activates the 18-electron complex $[FeL_2(NO)_2]$ towards substitution by σ donors and one-electron reduction activates the 17-electron complex $[FeXL(NO)_2]$ towards substitution by better π acceptors.

In the light of the reaction of **1b**$^+$ with iodide ion it is possible that the reaction between **1b** and I_2 to give $[FeI(PPh_3)(NO)_2]$ proceeds *via* one-electron oxidation followed by substitution of PPh_3 by I^-. A similar process has been proposed[20] for the oxidative addition of I_2 to $[Fe(CO)_3(PPh_3)_2]$, to give $[FeI_2(CO)_3(PPh_3)]$, where the first step is the formation of

Table 2 Selected bond lengths (Å) and angles (°) for the complexes $[Fe(PPh_3)_2(NO)_2]^z$

	$z = 0$[a]	$z = +1$[b]
Fe–P	2.267(2)	2.362(1)
Fe–N	1.650(7)	1.661(4)
N–O	1.190(10)	1.160(6)
P–C_{av}[c]	1.842(7)	1.811(5)
C–P–C_{av}	103.1(3)	106.3(2)
N–Fe–N	123.8(4)	113.5(3)
O···Fe···O	122.4	102.2
Fe–N–O	178.2(7)	166.2(4)
P–Fe–P	111.9(1)	123.1(1)
P–Fe–N_{av}	105.4(2)	105.7(2)

[a] Data from ref. 17. [b] As the PF_6^- salt. [c] The error given for the mean values is the largest individual standard deviation in the set of values averaged.

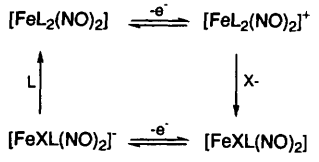

Scheme 1

the 17-electron cation $[Fe(CO)_3(PPh_3)_2]^+$. Complex **1b**$^+$ also reacts with 2 equivalents of Cl^- to give $[FeCl_2(NO)_2]^-$[21] though an excess of iodide ion is required to replace both phosphine ligands to give $[FeI_2(NO)_2]^-$.

Cation **1b**$^+$ reacts with an excess of $OPPh_3$ in thf at *ca.* −15 °C to give a purple solution from which violet microcrystals of $[Fe(OPPh_3)(PPh_3)(NO)_2][PF_6]$ [**3**]PF_6 can be isolated in moderate yield (Table 1). The IR spectrum of complex **3**$^+$ shows two nitrosyl peaks with relative intensities similar to those of **1b**$^+$, implying a similar tetrahedral structure, but at lower wavenumber in accord with the presence of the σ donor phosphine oxide ligand. The C, H and N analyses of **3**$^+$ are in good agreement with the formulation given. However, IR spectroscopy in CH_2Cl_2 (and cyclic voltammetry and ESR spectroscopy, see below) showed the presence of a small amount of **1b**$^+$ in all isolated samples of the $[PF_6]^-$ salt of **3**$^+$. It is not clear whether these peaks are due simply to residual **1b**$^+$ or to its formation by partial disproportionation of **3**$^+$ in solution. However, unlike **1b**$^+$, **3**$^+$ is stable in polar solvents such as thf [ν(NO) 1806m, 1743s cm^{-1}] and the former seems more likely.

The cyclic voltammogram of cation **3**$^+$ also differs from that of **1b**$^+$ in showing a reduction wave which is only partially reversible [$(E_p)_{red}$ = −0.25 V at a scan rate of 200 mV s^{-1}; i_{ox}/i_{red} = 0.66 at 200 mV s^{-1}, 0.88 at 1 V s^{-1}]. The apparent instability of the 18-electron complex **3**, even on the time-scale of cyclic voltammetry, may be due to the inability of the poorer π acceptor, $OPPh_3$, to stabilise the lower oxidation state. That the phosphine oxide is a poorer π acceptor (better σ donor) than PPh_3 is underlined by the more negative reduction potential of **3**$^+$ relative to that of **1b**$^+$.

As noted above, the cyclic voltammogram of **3**$^+$ shows the presence of small amounts (*ca.* 5%) of **1b**$^+$; a wave centred at *ca.* 0.40 V was detectable even when the reduction wave of **3**$^+$ (at −0.25 V) was not scanned. It is more noteworthy, however, that if the wave at −0.25 V is scanned the peak centred at 0.40 V becomes significantly larger, suggesting the formation of **1b** by the disproportionation of **3**.

In spite of the small amounts of **1b**$^+$ apparently present in solutions of **3**$^+$, pure crystals of the $[PF_6]^-$ salt of the latter were grown from thf–*n*-hexane and studied by X-ray

crystallography. The molecular structure of the cation is shown in Fig. 2 and selected bond lengths and angles are given in Table 3. The cation shows approximately tetrahedral co-ordination at iron and near linear nitrosyl ligands as expected. The distortions from tetrahedral geometry at iron are, however, notable; the L–Fe–L angles involving the triphenylphosphine ligand (average 102°) are systematically smaller than the others (average 116°). This distortion leads to a geometry at iron which is approaching pseudo-trigonal bipyramidal with the PPh_3 ligand in one apical site, the other apical site vacant and the $OPPh_3$ and nitrosyl ligands occupying equatorial sites. This is in contrast to the more irregular geometry of the only other tetrahedral tertiary phosphine–tertiary phosphine oxide complex whose crystal structure is known,[22] namely the Mn^{II} species $[MnI_2(OPMePh_2)(PMePh_2)]$, in which bond angles at Mn lie in the range 97.2–117.7°.

Complex $\mathbf{3}^+$ is also formed, but only very slowly, on passing gaseous O_2 through $\mathbf{1b}^+$ in CH_2Cl_2. This reaction contrasts markedly with that between $[\{Fe(\mu\text{-}X)(NO)_2\}_2]$ (X = Cl or I) and PPh_3 or $OPPh_3$ and O_2, which affords the bis(phosphine oxide) complex $[FeX(NO_3)_2(OPPh_3)_2]$,[23] and with that between $[\{Fe(\mu\text{-}Cl)(NO)_2\}_2]$, hexamethylphosphoramide (hmpa) and O_2, which gives, amongst other things, $[FeCl_2(NO_3)(hmpa)_2]$.[24]

The remaining PPh_3 ligand of $\mathbf{3}^+$ is not displaced even in the presence of an excess of $OPPh_3$. However, $[Fe(OPPh_3)_2(NO)_2][PF_6]$ [**4**]PF_6 (Table 1) is readily prepared from $[\{Fe(\mu\text{-}I)(NO)_2\}_2]$, $OPPh_3$ and $TlPF_6$. The cyclic voltammogram of $\mathbf{4}^+$ displays a completely irreversible reduction wave, even at 0 °C, [$(E_p)_{red} = -0.59$ V, scan rate = 200 mV s^{-1}], showing the neutral complex **4** to be unstable. Though the 17-electron cations $\mathbf{3}^+$ and $\mathbf{4}^+$ are stabilised by the σ-donor ligand $OPPh_3$ the 18-electron configuration requires better π acceptors, if only PPh_3. It is noteworthy that similar behaviour is observed for the complexes $[Cr(NO)L_2(cp)]^z$ ($z = 0$ or 1, L = two-electron donor). The 17-electron cations are stabilised by σ donors and the neutral complexes by π acceptors; only in the case of L = $P(OMe)_3$, however, both $[Cr(NO)L_2(cp)]$ and $[Cr(NO)L_2(cp)]^+$ are stable.[25]

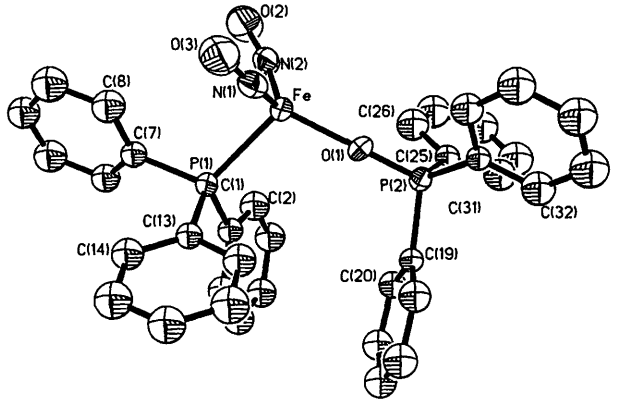

Fig. 2 Molecular structure of the cation of [**3**]PF_6 showing the atom labelling scheme. All hydrogen atoms have been omitted for clarity

Table 3 Selected bond lengths (Å) and angles (°) for $[Fe(OPPh_3)(PPh_3)(NO)_2][PF_6]$

Fe–P	2.369(5)	P–O	1.500(9)
Fe–O	1.913(9)	P(1)–C_{av}	1.798(14)
Fe–N_{av}	1.668(13)	P(2)–C_{av}	1.776(15)
N–O_{av}	1.171(18)		
P–Fe–O	106.7(3)	Fe–N–O_{av}	161.2(13)
N–Fe–N	112.3(6)	Fe–O–P	173.6(7)
P–Fe–N_{av}	99.4(6)	C–P(1)–C_{av}	105.7(7)
O–Fe–N_{av}	117.6(6)	C–P(2)–C_{av}	109.0(6)
O···Fe···O	98.1(6)	O–P(2)–C_{av}	110.0(6)

Chemical oxidation of 1a, 1c and 2

By contrast to the oxidation of **1b** those of **1** (L = PEt_3, L_2 = dppe) and **2** gave poorly defined products. Treatment of **1a** with a stoichiometric amount (1:1) of $[Fe(cp)_2][PF_6]$ in CH_2Cl_2 gave a new species with nitrosyl absorptions at 1809 and 1759 cm^{-1}. The increase in ν(NO) (*ca.* 110–115 cm^{-1}) (*cf.* **1a**) is comparable with that observed on oxidation of **1b** and on this basis the new species is assumed to be $\mathbf{1a}^+$ (an assumption supported by ESR spectroscopy, see below). However, on adding *n*-hexane to the reaction mixture a dark brown oil was formed the IR spectrum of which revealed a mixture of $\mathbf{1a}^+$ and another dinitrosyl [ν(NO) (CH_2Cl_2) 1789ms, 1737s cm^{-1}]; both species decomposed before further characterisation was possible.

The reaction of **1c** with $[NO]^+$ in CH_2Cl_2 gave a dark brown solution, the IR spectrum of which was again consistent with the formation of $\mathbf{1c}^+$ [ν(NO) (CH_2Cl_2) 1815m, 1762s cm^{-1}]. However, the reactions of **1c** with $[N(C_6H_4Br\text{-}p)_3][PF_6]$ and with ferrocenium ion appeared to give different species [ν(NO) 1813m, 1750s and 1824m, 1771s cm^{-1} respectively]. None of these species was isolable although the ESR spectrum of that generated by the *in situ* oxidation of **1c** with ferrocenium ion is discussed below. The reaction between **1c** and $[N_2C_6H_4F\text{-}p][PF_6]$ resulted in insertion of the arenediazo group into one Fe–P bond, giving[26] $[Fe\{PPh_2CH_2CH_2P(Ph)_2NN(C_6H_4F\text{-}p)\}(NO)_2][PF_6]$ rather than $\mathbf{1c}^+$.

Attempts to generate $\mathbf{2}^+$ from **2** also met with little success. Treatment of **2** with $[NO]^+$, $[N_2C_6H_4F\text{-}p]^+$, $[N(C_6H_4Br\text{-}p)_3]^+$ or $[Fe(cp)_2]^+$ led to rapid decomposition. Exhaustive controlled potential electrolysis of **2** at 0.50 V resulted in the consumption of *ca.* 0.9 electrons per molecule, in agreement with the proposal of one-electron oxidation, but $\mathbf{2}^+$ was not detected in the cyclic voltammogram of the electrolysed solution.

The reaction of **2** with 1 equivalent of I_2 in CH_2Cl_2 gave a green solution, the IR spectrum of which [ν(NO) 1793m, 1739s cm^{-1}] was virtually identical to that of the species believed to be $[FeI(\eta^1\text{-dppm})(NO)_2]$. Addition of less than a stoichiometric amount of I_2 gave mixtures containing only **2** and $[FeI(NO)_2(\eta^1\text{-dppm})]$, with no evidence for the formation of $[\{FeI(NO)_2\}_2(\mu\text{-dppm})]$ as an intermediate.

ESR spectra of 17-electron complexes

Second-derivative ESR spectra of $\mathbf{1b}^+$, $\mathbf{3}^+$ and $\mathbf{4}^+$ in liquid CH_2Cl_2 solution are shown in Figs. 3(*a*)–5(*a*); the *g* values and ^{31}P and ^{14}N hyperfine coupling constants are given in Table 4. Each spectrum shows coupling to two ^{14}N and two ^{31}P nuclei, consistent with the approximate tetrahedral geometry established in the solid state by X-ray crystallography for $\mathbf{1b}^+$ and $\mathbf{3}^+$. Thus the spectra of $\mathbf{1b}^+$ and $\mathbf{4}^+$ [Figs. 3(*a*) and 5(*a*)] are 1:2:1 triplets of 1:2:3:2:1 quintets (coupling of the unpaired electron to two equivalent ^{31}P and to two equivalent ^{14}N nuclei); in these spectra, the ^{14}N coupling is approximately the same, but the ^{31}P coupling is considerably larger for PPh_3 than for $OPPh_3$. The spectrum of $\mathbf{3}^+$ [Fig. 4(*a*)] is a doublet of sextets [a large ^{31}P coupling (PPh_3) and smaller, approximately equal, couplings to ^{31}P ($OPPh_3$) and to two equivalent ^{14}N nuclei]. As noted above, small amounts of $\mathbf{1b}^+$ are present in samples of $\mathbf{3}^+$ so that a weak spectrum of the former is detectable in Fig. 4(*a*).

The widths of the high-field features in the isotropic spectrum of $\mathbf{3}^+$ are significantly broader than those of the low-field features, and there are also small linewidth variations within the ^{14}N quintet. Similar, albeit smaller, effects are seen in the spectra of $\mathbf{1b}^+$ and $\mathbf{4}^+$, suggesting linewidths dependent on the ^{31}P and ^{14}N nuclear spin quantum numbers, as shown by equation (1).[27] Because of overlap problems, direct measurement of the linewidths proved impossible. Accordingly, the experimental second-derivative spectra were analysed using a

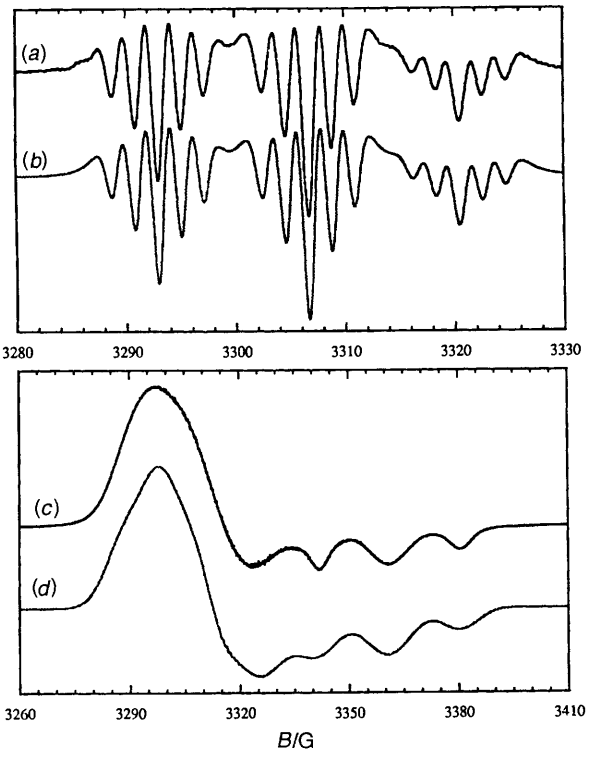

Fig. 3 ESR spectra of $[Fe(PPh_3)_2(NO)_2]^+$ **1b**$^+$: (*a*) second-derivative spectrum of a CH_2Cl_2 solution at 260 K (ν_o = 9.4450 GHz), (*b*) computer simulation using the parameters given in Table 4, (*c*) first-derivative spectrum of a frozen CH_2Cl_2–$C_2H_4Cl_2$ solution at 77 K (ν_o = 9.4755 GHz), (*d*) computer simulation using the parameters given in Table 4

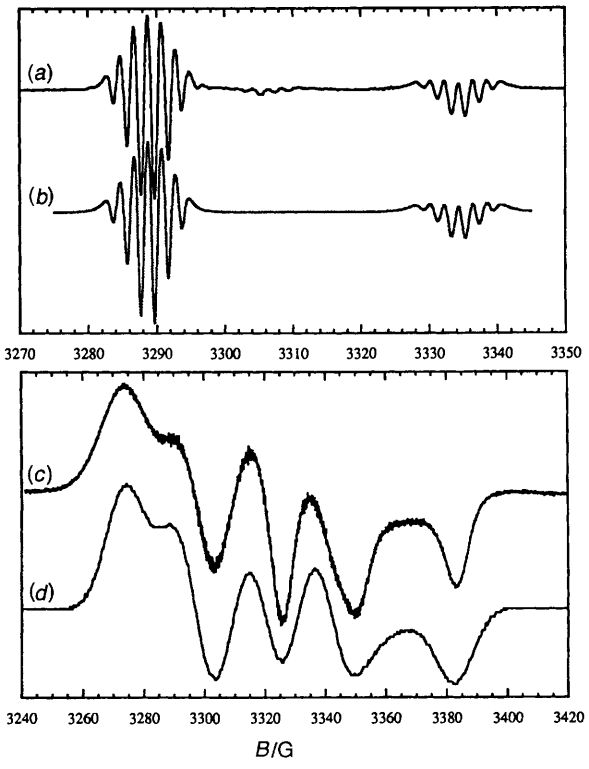

Fig. 4 ESR spectra of $[Fe(OPPh_3)(PPh_3)(NO)_2]^+$ **3**$^+$: (*a*) second-derivative spectrum of a CH_2Cl_2 solution at 220 K (ν_o = 9.4421 GHz), (*b*) computer simulation using the parameters given in Table 4, (*c*) first-derivative spectrum of a frozen CH_2Cl_2–$C_2H_4Cl_2$ solution at 77 K (ν_o = 9.4488 GHz), (*d*) computer simulation using the parameters given in Table 4

$$T_2^{-1} = \alpha + \sum_i (\beta_i m_i + \gamma_i m_i^2) + \sum_{i \neq j} \varepsilon_{ij} m_i m_j \qquad (1)$$

non-linear least-squares procedure.[28] The least-squares fitting procedure permitted more accurate determination of the hyperfine couplings than was possible by fitting of the line positions; in particular, the positions of features were accurate to third order in perturbation theory and the ^{14}N and ^{31}P ($OPPh_3$) couplings could be distinguished in the spectrum of **3**$^+$. In no case were the quadratic linewidth terms, γ_i or ε_{ij}, statistically significant. In all cases, the quality of fit was very good; spectra simulated using the fitted spin Hamiltonian and linewidth parameters, shown in Figs. 3(*b*)–5(*b*), are essentially superimposable on the experimental spectra. The least-squares spin Hamiltonian and linewidth parameters are given in Table 4. Note that the parameter uncertainties given reflect fitting precision rather than absolute accuracy, which was *ca.* 0.25%.

First-derivative ESR spectra of **1b**$^+$, **3**$^+$ and **4**$^+$ in frozen CH_2Cl_2–$C_2H_4Cl_2$ (1:1) solution at 77 K are also shown, in Figs. 3(*c*)–5(*c*). The spectrum of **1b**$^+$ [Fig. 3(*c*)] is approximately axial with the parallel feature a 1:2:1 triplet and the perpendicular region unresolved. The width and shape of the perpendicular feature can be accounted for by two overlapping *g* components, each an approximate 1:2:1 triplet, with $g = g_\perp \pm 0.003$, where $g_\perp$ and $A_\perp$ are computed from $\langle g \rangle$ and $g_\parallel$, $\langle A^P \rangle$ and $A_\parallel{}^P$. Careful examination of the parallel feature shows that the central component of the triplet is substantially broader than the outer components, suggesting that the ^{31}P nuclei are not exactly equivalent. Judging from the width, the two couplings differ by about ±15% from the average measured using the outer components, *i.e.*, $A_\parallel \approx 16$, 21×10^{-4} cm^{-1}. The perpendicular couplings may also be inequivalent, but because of the poor resolution, this cannot be proved. As we will see below, the principal axes of A_1 and A_2 are probably displaced from the *g*-matrix axes in equal and opposite directions. This effect does not lead to differences in the positions or widths of spectral features, but it does lead to an

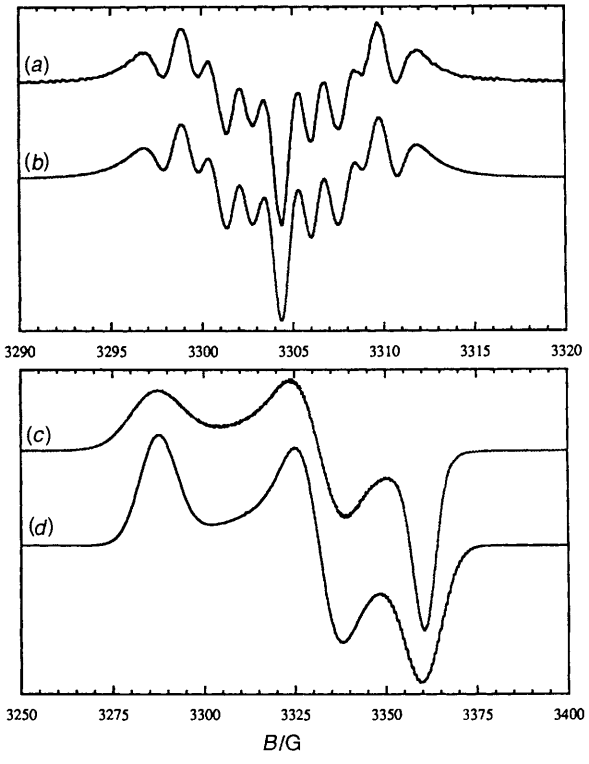

Fig. 5 ESR spectra of $[Fe(OPPh_3)_2(NO)_2]^+$ **4**$^+$: (*a*) second-derivative spectrum of a CH_2Cl_2 solution at 260 K (ν_o = 9.4402 GHz), (*b*) computer simulation using the parameters given in Table 4, (*c*) first-derivative spectrum of a frozen CH_2Cl_2–$C_2H_4Cl_2$ solution at 77 K (ν_o = 9.4756 GHz), (*d*) computer simulation using the parameters given in Table 4

Table 4 ESR spectroscopic data for the iron dinitrosyl complexes as their PF_6^- salts

Isotropic parameters (CH_2Cl_2 solution)

Complex	$\langle g \rangle$	Hyperfine couplings/G	Linewidth parameters/G
1b$^+$ $[Fe(PPh_3)_2(NO)_2]^+$	2.0370[a]	a^P = 13.792(2) a^N = 2.072(1)	α = 1.695(2) β_P = −0.180(3) β_N = 0.022(1)
3$^+$ $[Fe(OPPh_3)(PPh_3)(NO)_2]^+$	2.0332[b]	$a^{P(1)}$ = 45.66(1) $a^{P(2)}$ = 1.92(3) a^N = 1.998(6)	α = 1.510(6) $\beta_{P(1)}$ = −0.56(1) β_N = 0.027(3)
4$^+$ $[Fe(OPPh_3)_2(NO)_2]^+$	2.0372[a]	a^P = 2.827(4) a^N = 1.733(2)	α = 1.546(4) β_P = −0.015(4) β_N = 0.030(3)

Anisotropic parameters (77 K)

	g			$10^4 A^P/cm^{-1}$		
Complex	x	y	z	x	y	z
1b$^+$ $[Fe(PPh_3)_2(NO)_2]^+$	2.052	2.014	2.045	10.6[c]	18.2[d]	10.6[c]
3$^+$ $[Fe(OPPh_3)(PPh_3)(NO)_2]^+$	2.049	2.013	2.034	39.7	53.9	42.9
4$^+$ $[Fe(OPPh_3)_2(NO)_2]^+$	2.060	2.015	2.032	—	—	—

[a] Measured at 260 K. [b] Measured at 220 K. [c] Computed from $\langle A^P \rangle$ and A_y. [d] Average coupling.

underestimate of $(A_{\|})_{av}$, which may be as much as 10% greater than the value reported in Table 4.

The spectrum of **3**$^+$ [Fig. 4(*c*)] shows five features, the central line resulting from the overlap of two features; the spectrum is easily interpreted in terms of three g components, each with a doublet splitting. The spectrum of **4**$^+$ [Fig. 5(*c*)] shows three g components, but the hyperfine structure is unresolved. The resulting ESR parameters are given in Table 4 and computer simulations based on these parameters are shown in Figs. 3(*d*)–5(*d*).

Although no product could be isolated, the *in situ* oxidation of **1a** with $[Fe(cp)_2]^+$ gave an ESR spectrum very similar to that of **1b**$^+$; a triplet [$A(^{31}P)$ = 13.0 G] centred at g = 2.0382 suggests the formation of the cation **1a**$^+$. Similar oxidation of **1c**, however, resulted in the observation of a doublet [$A(^{31}P)$ = 47 G] centred at g = 2.0375. Despite careful exclusion of oxygen, and carrying out the reaction at low temperature (−78 °C), no evidence for the triplet expected for **1c**$^+$ was obtained. No further coupling, to ^{14}N or ^{31}P, was resolved but the similarity between the doublet spectrum and that of **4**$^+$ suggests the formation of the insertion product $[Fe\{OPPh_2CH_2CH_2PPh_2\}(NO)_2]^+$; such an insertion product would be related to $[Fe\{PPh_2CH_2CH_2P(Ph)_2NN(C_6H_4F\text{-}p)\}(NO)_2]^+$ [26] which is formed when **1c** reacts with $[N_2\text{-}C_6H_4F\text{-}p]^+$.

EHMO calculations on, and interpretation of ESR parameters for, $[Fe(PPh_3)_2(NO)_2]^+$ and $[Fe(OPPh_3)(PPh_3)(NO)_2]^+$

Summerville and Hoffmann[18] have carried out EHMO calculations on the general class of four-co-ordinate metal complexes $[MX_2Y_2]$ including dinitrosyls (*i.e.* Y = NO) the results of which will be discussed further below. However, in order to assist interpretation of the ESR spectra of the new complexes decribed herein, additional EHMO calculations were carried out specifically for $[Fe(PH_3)_2(NO)_2]$ and $[Fe(OPH_3)(PH_3)(NO)_2]$ (the parameters used, and the detailed results of the calculations are given in SUP 57156). Molecular geometries were based on the crystal structures of **1b**$^+$ and **3**$^+$ with the z axis bisecting the N–Fe–N angle and these atoms defining the xz plane (see Fig. 6).

Phosphorus-31 hyperfine couplings. The isotropic ^{31}P couplings arise through a combination of direct interaction of P 3s spin density and polarisation of P 1s and 2s orbitals by spin density in Fe and P 3p orbitals. Although quantitative interpretation is not possible, the magnitude of a phosphine ^{31}P coupling is generally related to the proximity of the phosphorus atom to the lobes of the singly-occupied MO. Thus the ^{31}P couplings are smaller for $OPPh_3$ than for PPh_3, as expected. The extended-Hückel MO calculations suggest that the singly occupied molecular orbital (SOMO) for $[Fe(PH_3)_2(NO)_2]^+$ is primarily an Fe $d_{x^2-y^2}/d_{z^2}$ hybrid of a_1 symmetry (assuming C_{2v} molecular symmetry, see below), as expected from the work of Summerville and Hoffmann.[18] The SOMO has major lobes along the y axis [$\theta = \pm 90°$, as defined in Fig. 6(*a*)] and a distorted d_{z^2}-like doughnut in the xz plane [see Fig. 6(*c*)]. The SOMO calculated for $[Fe(OPH_3)(PH_3)(NO)_2]^+$ is a similarly shaped $d_{x^2-y^2}/d_{z^2}/d_{yz}$ hybrid with major lobes in the yz plane but displaced by 13° from the y axis [θ = 103° and −77°; see Fig. 6(*b*) and 6(*d*)]. The crystal structure of **1b**$^+$, transformed to the EHMO coordinate system, shows PPh_3 ligands very nearly in the yz plane at $\theta = \pm 109°$, *i.e.* 19° below the $\pm y$ axis and the predicted major lobes of the SOMO. Similarly, the crystal structure of **3**$^+$ shows the PPh_3 ligand in the yz plane at θ = 107°, only 4° below a predicted major lobe of the SOMO. Thus the PPh_3 ligand in **3**$^+$ is much closer to a lobe of the

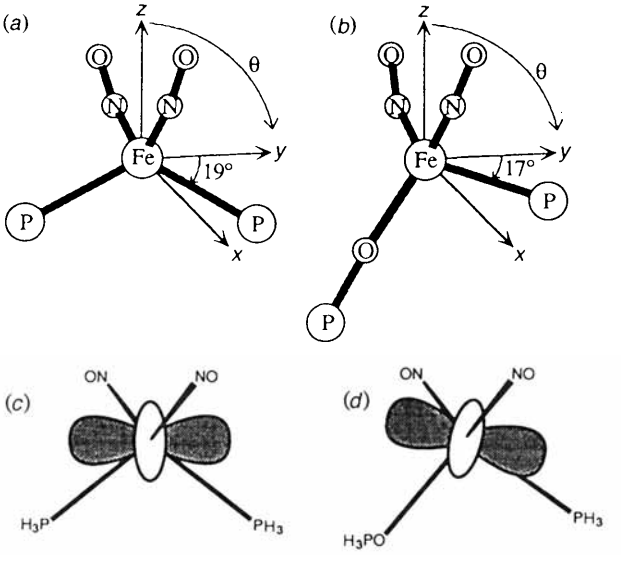

Fig. 6 Illustration of (*a*) $[Fe(PH_3)_2(NO)_2]^+$ and (*b*) $[Fe(OPH_3)(PH_3)(NO)_2]^+$, showing the coordinate system used in the discussion and for the EHMO calculations, and schematic illustrations of their respective SOMOs (*c*) and (*d*)

SOMO and would be expected to show a larger ^{31}P coupling than the PPh_3 ligands in $\mathbf{1b}^+$, as is observed.

In the frozen-solution spectrum, but not in the isotropic spectrum of $\mathbf{1b}^+$, the two ^{31}P nuclei are slightly non-equivalent. This effect suggests two equivalent minimum energy conformations, rapidly interconverted in liquid solution, which might represent distortions of the complex toward the trigonal bipyramidal-like geometry of $\mathbf{3}^+$. As we have seen, the ^{31}P coupling in these complexes is very sensitive to the angle between a major lobe of the SOMO and the Fe–P bond vector. Indeed, the observed difference in coupling, *ca.* ± 15%, might arise from a difference in this angle as small as 1–2°. In any case, the effect is too small to suggest a major distortion from the crystal structure.

The anisotropy in the ^{31}P hyperfine coupling arises through participation of P 3p orbitals in the SOMO, the major contributions to which are Fe 3d orbitals, as shown by equation (2) where the *a*'s are linear combination of atomic orbitals

$$|\mathrm{SOMO}\rangle = a_{x^2-y^2}|x^2 - y^2\rangle + a_{z^2}|z^2\rangle + a_{yz}|yz\rangle + b_y|y\rangle + b_z|z\rangle + \cdots \quad (2)$$

(LCAO) coefficients of Fe orbitals and the *b*'s are coefficients of P orbitals. Assuming that $3p_y$ and $3p_z$ orbitals are involved, the dipolar part of the hyperfine interaction matrix is given by equation (3) where P ($=305.9 \times 10^{-4}$ cm^{-1})[29] is the dipolar

$$A^{\mathrm{P}}_{\mathrm{dipolar}} = \tfrac{2}{5}P \begin{pmatrix} -b_y^2 - b_z^2 & 0 & 0 \\ 0 & 2b_y^2 - b_z^2 & -3b_yb_z \\ 0 & -3b_yb_z & -b_y^2 + 2b_z^2 \end{pmatrix} \quad (3)$$

interaction parameter. The matrix can be diagonalised by rotation about the *x* axis by the angle β, equation (4), to give an

$$\tan 2\beta = \frac{2b_yb_z}{b_y^2 - b_z^2} \quad (4)$$

$$A_{\parallel}^{\mathrm{P}} = \langle A^{\mathrm{P}}\rangle + \tfrac{4}{5}P(b_y^2 + b_z^2) \quad (5)$$

$$A_{\perp}^{\mathrm{P}} = \langle A^{\mathrm{P}}\rangle - \tfrac{2}{5}P(b_y^2 + b_z^2) \quad (6)$$

axial matrix with components given by equations (5) and (6). The spectrum of $\mathbf{3}^+$ can be refitted assuming an axial ^{31}P hyperfine matrix, as suggested by these equations, to give $A_{\parallel}^{\mathrm{P}} = 56.1 \times 10^{-4}$ cm^{-1}, $A_{\perp}^{\mathrm{P}} = 39.7 \times 10^{-4}$ cm^{-1}, $\beta = 22.5°$. These parameters give $b_y^2 = 0.038$, $b_z^2 = 0.006$, or a total phosphorus 3p contribution to the SOMO of 0.044. The much more poorly resolved spectrum of $\mathbf{1b}^+$ cannot be interpreted with this degree of refinement, but the apparent value of $A_{\parallel}^{\mathrm{P}}$ given in Table 4, together with $\langle A^{\mathrm{P}}\rangle$, leads to a P 3p spin density of 0.018.

The PH_3 phosphorus 3p spin densities from EHMO calculations on $[Fe(PH_3)_2(NO)_2]^+$ and $[Fe(OPH_3)(PH_3)(NO)_2]^+$ are 0.021 and 0.031, respectively, in satisfactory agreement with the ESR results. Furthermore, the contributions in both cases are $3p_y$ (major) and $3p_z$ (minor), suggesting that the largest and smallest hyperfine components (in the *g* matrix coordinate system) correspond to the g_{min} and g_{max} axes, which we have designated *y* and *x* respectively, in Table 4.

***g* Matrix components.** For a SOMO of the form given by equation (2), we expect *g* matrix components as shown by equations (7)–(10) where ζ is the spin-orbit coupling parameter for Fe, E_0 is the energy of the SOMO, and E_i is the energy and c^i_{xz} (for example) is the LCAO coefficient of d_{xz} in the *i*th MO. According to the EHMO calculations, the Fe contributions to the SOMO are $a_{x^2-y^2} > a_{z^2} > a_{yz}$ (with $a_{yz} = 0$ in the limit of C_{2v} symmetry). Thus $(g_{xx} - g_e)$, $(g_{yy} - g_e)$ and $(g_{zz} - g_e)$ are due primarily to spin–orbit coupling with MO's with d_{yz}, d_{xz} and d_{xy} character, respectively. Since $(a_{x^2-y^2} - \sqrt{3}a_{z^2})$ is small, $(g_{yy} - g_e)$ is expected to be small, and we assign g_{yy} to g_{min}, consistent with the assignment of the ^{31}P hyperfine axes. The cross-term, g_{yz}, which is proportional to $(a_{x^2-y^2} - \sqrt{3}a_{z^2})$ and requires coupling to molecular orbitals with both d_{xz} and d_{xy} character, is probably negligible. The EHMO calculations show that d_{xz} and d_{yz} character is spread over several molecular orbitals with energies both greater and less than that of the SOMO. The detailed calculation of *g* components is thus a hazardous enterprise, given the limitations of EHMO parameterisation.

$$g_{xx} = g_e + 2\zeta \sum_{i\neq 0} \frac{[a_{yz}(c^i_{x^2-y^2} + \sqrt{3}c^i_{z^2}) - (a_{x^2-y^2} + \sqrt{3}a_{z^2})c^i_{yz}]^2}{E_0 - E_i} \quad (7)$$

$$g_{yy} = g_e + 2\zeta \sum_{i\neq 0} \frac{[(a_{x^2-y^2} - \sqrt{3}a_{z^2})c^i_{xz} - a_{yz}c^i_{xy}]^2}{E_0 - E_i} \quad (8)$$

$$g_{zz} = g_e + 2\zeta \sum_{i\neq 0} \frac{[a_{x^2-y^2}c^i_{xy} - a_{yz}c^i_{xz}]^2}{E_0 - E_i} \quad (9)$$

$$g_{yz} = 2\zeta \sum_{i\neq 0} \frac{(a_{x^2-y^2}c^i_{xy} - a_{yz}c^i_{xz})[(a_{x^2-y^2} - \sqrt{3}a_{z^2})c^i_{xz} - a_{yz}c^i_{xy}]}{E_0 - E_i} \quad (10)$$

On the basis of ligand-field theory arguments, Bryar and Eaton[30] have suggested that the structures of paramagnetic iron dinitrosyl complexes can be deduced from the nature of the *g*-matrix components. In particular, they conclude that: (*i*) tetrahedral complexes should have three separate *g* components, all greater than g_e; (*ii*) complexes distorted toward trigonal bipyramidal (with a missing axial ligand) should have $g_\perp > g_\parallel \approx g_e$; and (*iii*) square planar (or tetragonally distorted octahedral) complexes should have $g_\parallel > g_\perp > g_e$. The *g* components for the present complexes are all quite similar [2.013–2.015, 2.032–2.045, 2.049–2.060] and, by the Bryar–Eaton criteria, all three complexes should be regarded as tetrahedral. In fact, as noted above, the crystal structure of $\mathbf{3}^+$ shows a significant distortion towards an axially vacant trigonal bipyramid, very similar to that observed[31] for $[FeCl(PPh_3)(NO)_2]$ for which Bryar and Eaton report an axial *g* matrix ($g_\parallel = 2.016$, $g_\perp = 2.046$), a result used to support the *g*-matrix structural criteria. The similarity in structure is better reflected by the ^{31}P couplings; $\langle a^{\mathrm{P}}\rangle = 49$ G for $[FeCl(PPh_3)(NO)_2]$,[30] very close to that for $\mathbf{3}^+$. While it might be appropriate to use *g*-matrix components to distinguish between gross structural differences, *e.g.* tetrahedral *vs.* square planar or tetragonally distorted octahedral, *g* components alone are not sufficient to detect distortions from tetrahedral stereochemistry, even when those distortions are quite large.

Linewidth parameters. To the extent that isotropic linewidths arise from incomplete averaging of anisotropies, the linewidth parameters, α, β_i, γ_i and ε_{ij}, are proportional, respectively, to $(g_\parallel - g_\perp)^2\tau_r$, $(g_\parallel - g_\perp)(A_\parallel{}^i - A_\perp{}^i)\tau_r$, $(A_\parallel{}^i - A_\perp{}^i)^2\tau_r$ and $(A_\parallel{}^i - A_\perp{}^i)(A_\parallel{}^j - A_\perp{}^j)\tau_r$, where τ_r is the rotational correlation time. The parameter α invariably includes other linewidth contributions, *e.g.* spin–rotation interaction and unresolved hyperfine structure. Given the small size of the isotropic couplings, it is not surprising that the quadratic terms γ_i and ε_{ij} are negligible [γ_P is probably non-negligible for $\mathbf{3}^+$, but $\gamma_P m_{P^2}$ contributes equally to all lines and so cannot be separated from α]. The first-order contributions to β_i are given by equation (11), where $g_\parallel = g_y$, $g_\perp = \frac{1}{2}(g_x + g_z)$, $\Delta g_\perp = g_x - g_z$, $A_\parallel{}^i = A_y{}^i$, $A_\perp{}^i = \frac{1}{2}(A_x{}^i + A_z{}^i)$, $\Delta A_\perp{}^i = A_x{}^i - A_z{}^i$, B_0 is the centre field of the spectrum, ω_0 is the angular microwave frequency, and the *A*'s are in units of cm^{-1}.[32] Substitution of the *g*- and

A^P-matrix anisotropies into equation (11), together with the

$$\beta_i = \frac{16\pi c B_0}{45\langle g\rangle}[(g_{\|} - g_{\perp})(A_{\|}{}^i - A_{\perp}{}^i) + \tfrac{3}{4}\Delta g_{\perp}\Delta A_{\perp}{}^i]\left(1 + \tfrac{3}{4}\frac{1}{1 + \omega_0^2\tau_r^2}\right)\tau_r \quad (11)$$

parameter β_P gives $\tau_r = 2.6 \times 10^{-10}$ s and 1.2×10^{-10} s, for $\mathbf{3}^+$ and $\mathbf{1b}^+$, respectively. The longer correlation time for $\mathbf{3}^+$ is consistent with the difference in temperatures of the experimental spectra.

Linewidth variations with the ^{14}N nuclear spin quantum number are much smaller, but the values of β_N are statistically significant. Since, within a ^{14}N multiplet, the widths increase with decreasing field, $\beta_N > 0$ if $\langle a^N\rangle > 0$. If the anisotropy of the ^{14}N coupling is due to dipolar coupling of a nitrogen $2p_y$ contribution to the SOMO, as suggested by EHMO calculations, $A_{\|}{}^N > A_{\perp}{}^N$. Since $g_{\|} < g_{\perp}$, β_N should be negative, implying $\langle a^N\rangle < 0$, *i.e.* the isotropic ^{14}N coupling arises through spin polarisation. The magnitudes of β_N, together with correlation times estimated above, give $A_{\|}{}^N - A_{\perp}{}^N \approx 1 \times 10^{-4}$ cm^{-1} for both $\mathbf{1b}^+$ and $\mathbf{3}^+$. This coupling suggests a nitrogen 2p spin density of about 0.02, given $P_N = 46.3 \times 10^{-4}$ cm^{-1}.[29] This is consistent with EHMO calculations which give nitrogen $2p_y$ SOMO contributions of 0.06 and 0.04 for $[Fe(PH_3)_2(NO)_2]$ and $[Fe(OPH_3)(PH_3)(NO)_2]$, respectively.

Bonding in $[ML_2(NO)_2]$ species

The oxidation of **1b** causes a substantial increase in the Fe–P distance [Δ(Fe–P) = 0.095 Å]. Oxidation also results in shorter P–C bonds in the cation [$\Delta(P\text{–}C_{av}) = -0.031$ Å] and an increase in the C–P–C angles [$\Delta(C\text{–}P\text{–}C_{av}) = 3.2°$]. These effects are consistent with significant Fe–P π back-bonding character in the HOMO of **1** and with a model for metal–phosphine π bonding in which the phosphine orbitals that contribute possess some P–C σ^* character.[33] This is entirely consistent with the EHMO calculations noted above on the model complex $[Fe(PH_3)_2(NO)_2]$. They suggest that the HOMO of **1b** is an orbital of a_1 symmetry (assuming C_{2v} molecular symmetry) which consists mainly of the metal $d_{x^2-y^2}$ (and d_{z^2}) together with some contribution from the phosphine π-acceptor orbitals which is manifested in small phosphorus 3p contributions to the HOMO. The metal dπ orbitals involved in π bonding to the stronger π-acceptor nitrosyl ligands lie at lower energies. The positive charge on the metal in $\mathbf{1b}^+$ reduces the amount of π back-donation to the nitrosyl π^* orbitals, *cf.* in **1b**. The consequent strengthening of the N–O bond results in a higher nitrosyl IR stretching frequency [$\Delta\nu$(NO) = *ca.* 100 cm^{-1}] for the cation. The effects on Fe–N and N–O distances are, however, rather small.

The effects of oxidation of **1b** to $\mathbf{1b}^+$ on the co-ordination geometry at iron are, by contrast, rather marked. Thus the interphosphine angle increases [Δ(P–Fe–P) = 11.2°] and the internitrosyl angle decreases [Δ(N–Fe–N) = −10.3°]. On the basis of EHMO calculations, consistent with those reported here, Summerville and Hoffmann[18] predicted that the X–M–X angle in $[MX_2Y_2]$ complexes will be greater than the Y–M–Y angle when X is a π acceptor and Y is a π donor (or a poorer π acceptor). They also suggested that, in the absence of other factors, the angle between better σ-donor ligands will be greater than that between poorer σ donors. If this is the case then the two effects will be in opposition in complexes in which X and Y are simultaneously π acceptors and σ donors. The geometry of **1b** implies that the π-bonding effects are dominant here, and in related cases noted by Summerville and Hoffmann,[18] since the angle between the superior π acceptors (the nitrosyls) is greater than that between the better σ donors (the phosphines).

The calculations of Summerville and Hoffmann also showed that the energy of the a_1 symmetry HOMO decreases as the interligand angle (X–M–X) closes, particularly when the ligands involved are not strong π acceptors. The HOMO of **1b** would therefore be expected to be stabilised by closing the angle between the phosphine ligands. The removal of an electron from the HOMO would reduce this driving force, thus allowing the interphosphine angle to increase, as is observed upon oxidation of **1b** to $\mathbf{1b}^+$.

Although the electronic model outlined here is in reasonable accord with the behaviour of the redox pair, **1b** and $\mathbf{1b}^+$, it fails to explain some details of related structural data. For example, the complex $[Co(PPh_3)_2(NO)_2]^+$[34] is isoelectronic and isostructural with **1b**. However, the charge on the ion would be expected to enhance σ donation by, and decrease π donation to, the ligands. The nitrosyl IR stretching frequencies are indeed high for the cobalt complex [ν(NO) (Nujol) 1836, 1784 cm^{-1}], showing that the amount of back bonding is considerably reduced. The phosphine C–P–C angles are larger [$C\text{–}P\text{–}C_{av}$ 105.2(2)°; $\Delta(C\text{–}P\text{–}C_{av}) = 2.1°$] and the P–C distances shorter [$P\text{–}C_{av}$ 1.818(5) Å; $\Delta(P\text{–}C_{av}) = -0.024$ Å] than in **1b**, consistent with π bonding to the phosphines also being reduced. It might thus be expected on the basis of the arguments above that the internitrosyl and interphosphine angles in $[Co(PPh_3)_2(NO)_2]^+$ would be smaller and larger respectively than those in **1b**. In fact, whilst there is a small increase in the interphosphine angle [P–Co–P 113.5(2)°; Δ(P–M–P) = 1.6°], the internitrosyl angle also increases [N–Co–N 136.7(4)°; Δ(N–M–N) = 12.9°]. Similar effects are observed in other isoelectronic pairs of dinitrosyl bis(triphenylphosphine) complexes,[35] and in the isoelectronic pair $[M(dppe)(NO)_2]^z$ (M = Fe, $z = 0$;[11] M = Co, $z = +1$).[36] These data suggest that the differences in geometry between **1b** and $\mathbf{1b}^+$ are not simply due to a change in the ratio of σ to π bonding on oxidation and that there is scope for further refinement of structure–bonding arguments in this area.

For the reasons given above it is possible that π bonding is more important in **1b** but that the enhanced hardness of the metal resulting from oxidation to $\mathbf{1b}^+$ causes σ-bonding effects to become dominant. That the phosphines are stronger σ donors than the nitrosyls might therefore also explain why the P–Fe–P angle is greater than the N–Fe–N angle in $\mathbf{1b}^+$. Steric factors may also be important in determining the geometries of **1b** and $\mathbf{1b}^+$. Although explanations of the behaviour of pseudo-tetrahedral dinitrosyl complexes have generally focused on electronic effects, it has been suggested that non-bonded repulsions within the M(NO)L units may have a crucial role in determining the geometry of these species.[37] In this case, whilst the requirements of the nitrosyls for Fe–N π bonding may force the phosphines together in **1b**, this restraint is weakened upon oxidation. The large steric demand of the bulky PPh_3 groups[38] would then act to open the interphosphine angle, at the same time forcing the nitrosyls closer together.

Another effect of the oxidation of **1b** is the bending of the nitrosyl ligands in the cation [Δ(Fe–N–O) = 12.0° (2σ = 2.2°)]. This is especially interesting as the ligands bend towards one another, with insignificant deviations from planarity of the $Fe(NO)_2$ unit. It has been noted previously that, for pseudo-tetrahedral dinitrosyl complexes, there is a linear correlation between the non-bonding O···M···O angle and the N–M–N bond angle.[35,39,40] These studies were based on a small number of structures (*e.g.* 13 in ref. 39) and were thus of reduced significance.[39] However, there are now 54 metal dinitrosyl fragments in structures at the Cambridge Structural Database.[41] (The relevant data, with references, are listed in SUP 57156.) The excellent linear correlation between their N–M–N and O···M···O angles (Pearson correlation coefficient = 0.982) is shown in Fig. 7. The equation of the line is $y = -87.76 + 1.675x$ (where y = O···M···O angle, x =

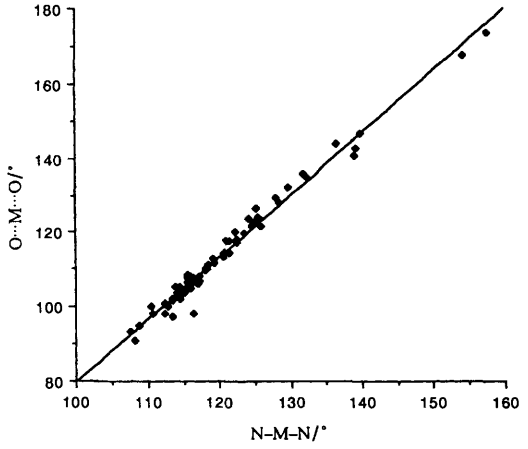

Fig. 7 Plot of the non-bonded angle O···M···O *vs.* the N–M–N bond angle for pseudo-tetrahedral dinitrosyl metal complexes

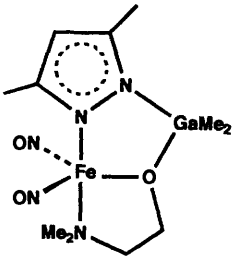

Fig. 8 Illustration of complex **5**

N–M–N angle). The correlation between the O···M···O and N–M–N angles suggests that the bending of the nitrosyl ligands is a property of the $M(NO)_2$ fragment as a whole, and not of the individual nitrosyl ligands. If the latter were the case then on simple steric grounds the O···M···O angle would be expected to be larger than or equal to the N–M–N angle. The distortion observed in these complexes would thus appear to be unrelated to the bending observed in those complexes where nitrosyl ligands act as one-electron donors.[42-44] If the bending in pseudo-tetrahedral dinitrosyl complexes were due to a degree of one-electron-donor character then it would be expected to be less in the more electron-deficient complexes, but more pronounced distortions are in fact observed in 17-electron than in 18-electron iron complexes. An elegant and successful explanation of the degree and direction of the bending as secondary functions of the internitrosyl angle has been proposed by Summerville and Hoffmann.[18] Their argument suggests that at larger N–M–N angles outwards distortion (increasing the O···M···O angle) of the two NO ligands is favoured since it reduces antibonding interactions between the NO lone pairs and the HOMO, while increasing bonding overlap between the HOMO and the NO π* orbitals.

Nature of paramagnetic iron dinitrosyl catalysts

The studies described above shed further light on the nature of previously described iron dinitrosyl complex catalysts.[6-8] The halide abstraction reactions of $[\{Fe(\mu\text{-}Cl)(NO)_2\}_2]$ with Ag^+ or Tl^+ salts in donor solvents such as acetone, thf or MeCN give solutions of cationic dinitrosyl complexes which catalyse the polymerisation of alkenes and dienes. On adding phosphines or phosphites to such solutions, new species are formed which show ESR spectra with well defined hyperfine coupling to phosphorus and the nitrosyl nitrogen atoms. For example, the addition of PPh_3 to an acetonitrile solution led to the observation of a doublet of quintets centred at $g = 2.0210$; the hyperfine coupling was assigned to the N atoms of two equivalent NO ligands [$A(^{14}N) = 3$ G] and to one P ligand [$A(^{31}P) = 54$ G]. A similar spectrum was observed when $[NO]^+$ was added to $[Fe(PPh_3)_2(NO)_2]$ in thf and when $[Fe(PPh_3)(NO)_3]^+$ was treated with thf.[7]

On the basis of such spectra, and of extended X-ray absorption fine structure (EXAFS)[45] studies and MO calculations,[6] the paramagnetic catalysts and their derivatives were formulated as five-co-ordinate 19-electron complexes $[FeL(L')_2(NO)_2]^+$ with trigonal bipyramidal structures. The observed hyperfine coupling patterns were explained by assuming that the unpaired electron interacts only with ligands bound in the equatorial plane. Thus, the doublet of *six* lines observed when $[Fe(dppe)(NO)_2]$ reacts with $[NO]^+$ in thf was assigned to the complex $[Fe(thf)(dppe)(NO)_2]^+$, with an equatorial phosphorus atom giving the large doublet coupling (55 G) and an axial phosphorus atom giving rise to a much smaller coupling similar to that with two equatorial nitrosyl nitrogen atoms (*ca.* 3 G) (thus leading to the sextet pattern).

Some support for the proposed trigonal bipyramidal structure is provided by the structural characterisation[46] of the paramagnetic iron dinitrosyl complex **5** (Fig. 8); although it appears to have a 19-electron configuration its ESR spectrum has not been reported. However, on the basis of the ESR spectroscopic studies reported herein, together with the structural analyses of $\mathbf{1b}^+$ and $\mathbf{3}^+$, we believe that the catalysts and their P-donor ligand derivatives are more likely to be tetrahedral 17-electron species. It is particularly noteworthy that the ESR parameters for $\mathbf{3}^+$ (Table 4) are very similar to those for the solution species prepared from $[Fe(dppe)(NO)_2]$ and $[NO]^+$ in thf,[6] suggesting the latter to be $[Fe\{OPPh_2CH_2CH_2PPh_2\}(NO)_2]^+$ where the six lines result from coupling to two nitrosyl N atoms and the P atom of the phosphine oxide. It is interesting that the ESR spectrum (doublet, $A = 50$ G, $g = 2.033$) of an incompletely characterised, air-sensitive complex formed in the reaction between $[\{FeCl(NO)_2\}_2(\mu\text{-dppe})]$ and 1 equivalent of dppe (or from $[\{Fe(\mu\text{-}Cl)(NO)_2\}_2]$ and 2 equivalents of dppe) 'can be taken to indicate that dppe has been partially oxygenated into $OPPh_2CH_2CH_2PPh_2$ so that coupling with the P(O) phosphorus atom is no longer detected'.[12] This species is most probably $[Fe\{OPPh_2CH_2CH_2PPh_2\}(NO)_2]^+$ rather than the proposed five-co-ordinate complex.

Conclusion

(*i*) The 17-electron cations $[FeL(L')(NO)_2]^+$ [L = L' = PPh_3, $\mathbf{1b}^+$; L = PPh_3, L' = $P(OPh)_3$, $\mathbf{3}^+$; L = L' = $P(OPh)_3$, $\mathbf{4}^+$] have been isolated as their $[PF_6]^-$ salts and fully characterised. The two series of iron dinitrosyl complexes, $[FeL_2(NO)_2]$ (18-electron) and $[FeX(L)(NO)_2]$ (17-electron) are linked by a 'square scheme' in which one-electron oxidation activates the former towards substitution by σ donors and one-electron reduction activates the latter towards substitution by better π acceptors.

(*ii*) A comparison of the structures of $\mathbf{1b}^+$ and **1b** suggests that oxidation is metal based and that the SOMO has M–P π bonding character. The iron atom shows C_{2v} local symmetry in both species. The changes in co-ordination geometry are broadly consistent with a bonding model proposed by Summerville and Hoffmann[18] for complexes $[MX_2Y_2]$.

(*iii*) The $M(NO)_2$ fragment shows a counterintuitive distortion in which the nitrosyl ligands bend towards one another, consistent with a database study of the geometries of a large number of metal dinitrosyl complexes and with the Summerville and Hoffmann[18] analysis.

(*iv*) The crystal structure analysis of $[\mathbf{3}]PF_6$ shows the cation to be distorted from tetrahedral geometry towards axially vacant trigonal bipyramidal co-ordination at iron. This geometry is consistent with the enhanced hyperfine coupling to the phosphine phosphorus atom observed in the ESR spectrum.

(*v*) Interpretation of the ESR parameters for $\mathbf{1b}^+$, $\mathbf{3}^+$ and $\mathbf{4}^+$

provides a very complete picture of the SOMO which is in good agreement with extended-Hückel MO calculations on the model complexes $[Fe(PH_3)_2(NO)_2]$ and $[Fe(OPH_3)(PH_3)(NO)_2]$. The magnitude of the isotropic ^{31}P hyperfine coupling is found to provide a sensitive measure of distortion from tetrahedral stereochemistry, more reliable than the criteria based on *g*-matrix components proposed by Bryar and Eaton.[30]

(*vi*) On the basis of structural and ESR studies on **1b**$^+$, **3**$^+$, *etc.*, iron dinitrosyl catalysts previously formulated as five-co-ordinate species are more likely to have near tetrahedral four-co-ordinate geometry.

Experimental

The preparation, purification and reactions of the complexes described were carried out under an atmosphere of dry nitrogen or argon using dried, distilled and deoxygenated solvents; reactions were monitored by IR spectroscopy where appropriate. Unless stated otherwise complexes were purified by dissolution in CH_2Cl_2 or thf, filtration of the solution through Celite, addition of *n*-hexane to the filtrate and reduction of the volume of the mixture *in vacuo* to induce precipitation. The compounds $[\{Fe(\mu\text{-}I)(NO)_2\}_2]$,[47] $[Fe(CO)_2(NO)_2]$,[48] $[Fe(cp)_2][PF_6]$[49] and $[Co(cp)_2]$[50] were prepared by published methods; $[Fe(PPh_3)_2(NO)_2]$[9] and $[Fe(dppe)(NO)_2]$[11,51] were prepared by modifications of the published methods. Infrared spectra were recorded on a Nicolet 5ZDX FT spectrometer, X-band ESR spectra on a Bruker ESP-300E spectrometer equipped with a Bruker variable-temperature accessory and a Hewlett Packard 5350B microwave frequency counter. The field calibration was checked by measuring the resonance of the diphenylpicrylhydrazyl (dpph) radical before each series of spectra. Proton NMR spectra were recorded on a JEOL GX270 spectrometer with $SiMe_4$ as an external reference. Electrochemical studies were carried out using an EG&G model 273 potentiostat in conjunction with a three-electrode cell. For cyclic voltammetry the auxiliary electrode was a platinum wire and the working electrode a platinum disc. The reference was an aqueous saturated calomel electrode (SCE) separated from the test solution by a fine-porosity frit and an agar bridge saturated with KCl. Solutions were 0.1×10^{-3} mol dm^{-3} in the test compound and 0.1 mol dm^{-3} in $[NBu_4][PF_6]$ as the supporting electrolyte. Under these conditions, $E^{\circ\prime}$ for the one-electron oxidation of $[Fe(cp)_2]$ and $[Fe(\eta\text{-}C_5Me_5)_2]$, added to the test solutions as internal calibrants, are 0.47 and −0.09 V respectively in CH_2Cl_2 and 0.39 and −0.12 V respectively in MeCN. Microanalyses were carried out by the staff of the Microanalytical Service of the School of Chemistry, University of Bristol.

Syntheses

Bis(triethylphosphine)dinitrosyliron, $[Fe(PEt_3)_2(NO)_2]$ 1a. To a stirred solution of PEt_3 (1 cm^3, 6.77 mmol) in toluene (50 cm^3) was added $[Fe(CO)_2(NO)_2]$ (375 μl, 3.39 mmol). After 0.5 h IR spectroscopy showed the formation of $[Fe(CO)(PEt_3)(NO)_2]$ and the absence of the dicarbonyl starting material. After heating the solution under reflux for 1 h, the reaction mixture was evaporated to dryness. The residue was then chromatographed on an *n*-hexane–alumina column, eluting with thf–*n*-hexane (1 : 10); the brown eluate was evaporated to dryness and the residue was crystallised from diethyl ether–*n*-hexane (1 : 1) at −78 °C to give black needles of the product, yield 620 mg (52%). The compound decomposes slowly under nitrogen at low temperatures; it dissolves in polar and non-polar solvents to give air-sensitive solutions.

Bis(triphenylphosphine)dinitrosyliron, $[Fe(PPh_3)_2(NO)_2]$ 1b. To a stirred solution of $[\{Fe(\mu\text{-}I)(NO)_2\}_2]$ (0.64 g, 1.32 mmol) and PPh_3 (1.39 g, 5.31 mmol) in toluene (50 cm^3) was added $[Co(cp)_2]$ (0.53 g, 2.80 mmol) in toluene (100 cm^3). After 5 min the brown solution was filtered through Celite and reduced to low volume *in vacuo*; addition of *n*-hexane gave a brown solid which was purified from CH_2Cl_2–*n*-hexane to give brown microcrystals of the product, yield 0.47 g (28%). The compound is moderately stable in air and dissolves in solvents such as CH_2Cl_2 and thf to give moderately air-sensitive solutions.

[1,2-Bis(diphenylphosphino)ethane]dinitrosyliron, $[Fe(dppe)(NO)_2]$ 1c. To a stirred solution of $[\{Fe(\mu\text{-}I)(NO)_2\}_2]$ (3.35 g, 7.0 mmol) in toluene (100 cm^3) was added dppe (7.24 g, 18.2 mmol). The brown solution was filtered through Celite and reduced to low volume *in vacuo*, addition of *n*-hexane giving a brown solid. The solid was then chromatographed on an *n*-hexane–alumina column, eluting with a 1 : 1 mixture of CH_2Cl_2–*n*-hexane. Further purification, from CH_2Cl_2–*n*-hexane, gave red-brown microcrystals, yield 4.42g (62%).

Bis-μ-[bis(diphenylphosphino)methane]tetranitrosyldiiron–tetrahydrofuran, $[\{Fe(\mu\text{-dppm})(NO)_2\}_2]$·thf 2. To a stirred solution of $[\{Fe(\mu\text{-}I)(NO)_2\}_2]$ (0.40 g, 0.82 mmol) and dppm (0.63 g, 1.63 mmol) in toluene (100 cm^3) was added $[Co(cp)_2]$ (0.31 g, 1.63 mmol). The pale brown solution was filtered through Celite and evaporated to dryness. The residue was chromatographed on an *n*-hexane–alumina column, eluting with CH_2Cl_2–*n*-hexane (1 : 10), and then purified from CH_2Cl_2–*n*-hexane and subsequently from thf–*n*-hexane to give ochre microcrystals, yield 0.48 g (54%). The compound is stable under nitrogen at low temperatures and dissolves in CH_2Cl_2 or thf to give slightly air-sensitive solutions.

Bis(triphenylphosphine)dinitrosyliron hexafluorophosphate, $[Fe(PPh_3)_2(NO)_2][PF_6]$ [1b]PF_6. To a stirred solution of $[Fe(PPh_3)_2(NO)_2]$ (0.45 g, 0.73 mmol) in CH_2Cl_2 (50 cm^3) was added $[Fe(cp)_2][PF_6]$ (0.23 g, 0.70 mmol). After 15 min the dark brown solution was filtered though Celite, *n*-hexane was added to the filtrate and the volume of the mixture was reduced *in vacuo* to induce precipitation. Purification of the precipitate from CH_2Cl_2–*n*-hexane gave black microcrystals, yield 0.37 g (66%). The compound is stable at low temperature under nitrogen; it dissolves in CH_2Cl_2 to give air-sensitive solutions and decomposes immediately in more polar solvents such as thf.

(Triphenylphosphine oxide)(triphenylphosphine)dinitrosyliron hexafluorophosphate, $[Fe(OPPh_3)(PPh_3)(NO)_2][PF_6]$ [3]PF_6. To a stirred solution of $OPPh_3$ (0.48 g, 1.73 mmol) in thf (40 cm^3) at *ca.* −15 °C (ice–salt bath) was added $[Fe(PPh_3)_2(NO)_2][PF_6]$ (0.27 g, 0.34 mmol). After 15 min the purple solution was filtered through Celite and cold toluene was added to induce precipitation. The product was washed with toluene and *n*-hexane and purified from thf–*n*-hexane to give violet microcrystals, yield 0.14 g (51%). The compound is stable under nitrogen at low temperature; it dissolves in CH_2Cl_2 to give air-sensitive solutions.

Bis(triphenylphosphine oxide)dinitrosyliron hexafluorophosphate, $[Fe(OPPh_3)_2(NO)_2][PF_6]$ [4]PF_6. To a stirred solution of $[\{Fe(\mu\text{-}I)(NO)_2\}_2]$ (0.20 g, 0.41 mmol) in CH_2Cl_2 (50 cm^3) at *ca.* −15 °C (ice–salt bath) was added $OPPh_3$ (1.20 g, 4.32 mmol) and $TlPF_6$ (0.60 g, 1.72 mmol). After 10 min the solution was filtered through Celite and cold toluene was added to induce precipitation. Purification from CH_2Cl_2–*n*-hexane gave a beige powder, yield 0.34 g (50%). The compound decomposes even under nitrogen at low temperature. It is soluble in CH_2Cl_2 or thf to give air-sensitive solutions.

Crystal-structure determinations of [1b]PF_6 and [3]PF_6

Many of the details of the structure analyses carried out on **1b**$^+$

Table 5 Crystal-structure determinations

Compound	[**1b**]PF_6	[**3**]PF_6
Formula	$C_{36}H_{30}F_6FeN_2O_2P_3$	$C_{36}H_{30}F_6FeN_2O_3P_3$
M	785.4	801.4
Crystal system	Monoclinic	Triclinic
Space group	$C2/c$ (no. 15)	$P\bar{1}$ (no. 2)
a/Å	18.728(6)	9.655(4)
b/Å	8.356(2)	10.169(4)
c/Å	24.092(7)	19.471(7)
α/°		85.88(3)
β/°	104.48(2)	77.50(3)
γ/°		88.81(3)
U/Å^3	3650(2)	1861.5(13)
Z	4	2
D_c/g cm^{-3}	1.43	1.43
$F(000)$	1604	818
μ(Mo-Kα)/mm^{-1}	0.61	0.60
Crystal dimensions/mm	0.6 × 0.3 × 0.2	0.51 × 0.37 × 0.03
2θ range/°	4–54	4–45
Scan method	Wyckoff, ω	Wyckoff, ω
Scan width (ω/°)	0.8	0.6
Total data	4266	4862
Unique data	3863 (R_{int} = 0.020)	4862
Observed data (n.o.) [$F^2 > 2\sigma(F^2)$]	1992	2111
Min., max. transmission coefficients	0.769, 0.863	0.426, 0.486
Least squares variables (n.v.)	228	280
R*	0.048	0.084
R'*	0.045	0.078
S*	1.16	1.63
g	0.0005	0.0005
Final difference map features/e Å^{-3}	+0.32, −0.26	+0.51, −0.40

* $R = \Sigma|\Delta|/\Sigma|F_o|$; $R' = [\Sigma w\Delta^2/\Sigma wF_o^2]^{\frac{1}{2}}$; $S = [\Sigma w\Delta^2/(\text{n.o.} - \text{n.v.})]^{\frac{1}{2}}$; $\Delta = F_o - F_c$; $w = [\sigma_c^2(F_o) + gF_o^2]^{-1}$, $\sigma_c^2(F_o)$ = variance in F_o due to counting statistics.

and **3**$^+$ are listed in Table 5. X-Ray diffraction measurements on single crystals mounted in thin-walled glass capillaries were made with graphite-monochromated Mo-Kα X-radiation (λ = 0.710 73 Å) using Siemens four-circle R3m diffractometers. Cell dimensions for each analysis were determined from the setting angle values of centred reflections in the range $15 < 2\theta < 30°$.

Intensity data were collected for unique portions of reciprocal space and corrected for Lorentz and polarisation effects, long-term intensity fluctuations and for absorption effects (on the basis of azimuthal scan data). The structures were solved by direct methods, and refined by full-matrix least squares against F. All non-hydrogen atoms were refined without positional constraints. For **1b**$^+$ all non-hydrogen atoms were assigned anisotropic displacement parameters while for **3**$^+$ only the atoms heavier than carbon were refined anisotropically. In both analyses all hydrogen atoms were assigned fixed isotropic displacement parameters and were constrained to ideal geometries (C–H 0.96 Å). Final difference syntheses showed no chemically significant features, the largest maxima being close to the metal atoms. Refinements converged smoothly to residuals given in Table 5.

All calculations were made with programs of the SHELXTL[52] system as implemented on a Siemens R3m/V structure-determination system. Complex neutral-atom scattering factors were taken from ref. 53.

Atomic coordinates, thermal parameters, and bond lengths and angles have been deposited at the Cambridge Crystallographic Data Centre (CCDC). See Instructions for Authors, *J. Chem. Soc., Dalton Trans.*, 1996, Issue 1. Any request to the CCDC for this material should quote the full literature citation and the reference number 186/146.

Acknowledgements

We thank the SERC for Research Studentships (to F. L. A. and N. C. B.) and for funds to purchase an ESR spectrometer. We thank Dr. G. M. Rosair for assistance with one of the crystal-structure analyses.

References

1 See, for example, B. F. G. Johnson and J. A. McCleverty, *Prog. Inorg. Chem.*, 1966, **7**, 277; N. G. Connelly, *Inorg. Chim. Acta Rev.*, 1972, **6**, 47; P. N. Hawker and M. V. Twigg, in *Comprehensive Coordination Chemistry*, eds. G. Wilkinson, R. D. Gillard and J. A. McCleverty, Pergamon, Oxford, 1987, vol. 4, ch. 44.1, p. 1187.
2 W. Hieber and H. Führling, *Z. Anorg. Allg. Chem.*, 1970, **373**, 48.
3 D. Ballivet, C. Billard and I. Tkatchenko, *Inorg. Chim. Acta*, 1977, **25**, L58.
4 R. E. Dessy, J. C. Charkoudian and A. L. Rheingold, *J. Am. Chem. Soc.*, 1972, **94**, 738.
5 M. F. Lappert, J. J. MacQuitty and P. L. Pye, *J. Chem. Soc., Dalton Trans.*, 1981, 1583.
6 D. Ballivet-Tkatchenko, J. Vincent-Vaucquelin, B. Nickel and A. Rassat, in *Paramagnetic Organometallic Species in Activation, Selectivity, Catalysis*, eds. M. Chanon, M. Julliard and J. C. Poite, Kluwer Academic Publishers, Holland, 1989.
7 D. Ballivet-Tkatchenko, B. Nickel, A. Rassat and J. Vincent-Vaucquelin, *Inorg. Chem.*, 1986, **25**, 3497.
8 D. Ballivet-Tkatchenko, C. Billard and A. Revillon, *J. Polym. Sci., Polym. Chem. Ed.*, 1981, **19**, 1697.
9 L. Malatesta and A. Araneo, *J. Chem. Soc.*, 1957, 3803.
10 S. Pignataro, G. Distefano and A. Foffani, *J. Am. Chem. Soc.*, 1970, **92**, 6425.
11 H. Li Kam Wah, M. Postel and M. Pierrot, *Inorg. Chim. Acta*, 1989, **165**, 215.
12 P. Guillaume, H. Li Kam Wah and M. Postel, *Inorg. Chem.*, 1991, **30**, 1828.
13 K. S. Chong, S. J. Rettig, A. Storr and J. Trotter, *Can. J. Chem.*, 1979, **57**, 3119.
14 V. A. Trumpy, T. A. Oriskovich and S. Schreiner, *Inorg. Chim. Acta*, 1993, **205**, 149.
15 R. H. Morris, K. A. Earl, R. L. Luck, N. J. Lazarowych and A. Sella, *Inorg. Chem.*, 1987, **26**, 2674 and refs. therein.

16 P. Hydes, J. A. McCleverty and D. G. Orchard, *J. Chem. Soc. A*, 1971, 3660.
17 V. G. Albano, A. Araneo, P. L. Bellon, G. Ciani and M. Manassero, *J. Organomet. Chem.*, 1974, **67**, 413.
18 R. H. Summerville and R. Hoffmann, *J. Am. Chem. Soc.*, 1976, **98**, 7240.
19 M. J. Therien, C.-L. Ni, F. C. Anson, J. G. Osteryoung and W. C. Trogler *J. Am. Chem. Soc.*, 1986, **108**, 4037.
20 P. K. Baker, N. G. Connelly, B. M. R. Jones, J. P. Maher and K. R. Somers, *J. Chem. Soc., Dalton Trans.*, 1980, 579.
21 D. Gwost and K. G. Caulton, *Inorg. Chem.*, 1973, **12**, 2095; N. G. Connelly and C. Gardner, *J. Chem. Soc., Dalton Trans.*, 1976, 1525.
22 S. M. Godfrey, C. A. McAuliffe, P. T. Ndifon and R. G. Pritchard, *J. Chem. Soc., Dalton Trans.*, 1993, 3373.
23 F. Tomi, H. Li Kam Wah and M. Postel, *New. J. Chem.*, 1988, **12**, 289.
24 H. Li Kam Wah, M. Postel and F. Tomi, *Inorg. Chem.*, 1989, **28**, 233.
25 P. Legzdins, W. S. McNeil, R. J. Batchelor and F. W. B. Einstein, *J. Am. Chem. Soc.*, 1994, **116**, 6021.
26 F. L. Atkinson, N. G. Connelly, J. G. Crossley and A. G. Orpen, *J. Chem. Soc., Dalton Trans.*, 1994, 1161.
27 G. K. Fraenkel, *J. Phys. Chem.*, 1967, **71**, 139.
28 L. V. Casagrande, T. Chen, P. H. Rieger, B. H. Robinson, J. Simpson and S. J. Visco, *Inorg. Chem.*, 1984, **23**, 2019.
29 J. R. Morton and K. F. Preston, *J. Magn. Reson.*, 1978, **30**, 577.
30 T. R. Bryar and D. R. Eaton, *Can. J. Chem.*, 1992, **70**, 1917.
31 J. Kopf and J. Schmidt, *Z. Naturforsch., Teil B*, 1975, **30**, 149.
32 R. Wilson and D. Kivelson, *J. Chem. Phys.*, 1966, **44**, 154.
33 S.-X. Xiao, W. C. Trogler, D. E. Ellis and Z. Berkovitch-Zellin, *J. Am. Chem. Soc.*, 1983, **105**, 7033; D. S. Marynick, *J. Am. Chem. Soc.*, 1984, **106**, 4064; A. G. Orpen and N. G. Connelly, *Organometallics*, 1990, **9**, 1206; B. J. Dunne, R. B. Morris and A. G. Orpen, *J. Chem. Soc., Dalton Trans.*, 1991, 653.
34 B. E. Reichert, *Acta Crystallogr., Sect. B.*, 1976, **32**, 1934.
35 G. Le Borgne, L. Mordenti, J. G. Riess and J.-L. Roustan, *New J. Chem.*, 1986, **10**, 97 and refs. therein.
36 J. A. Kaduk and J. A. Ibers, *Inorg. Chem.*, 1977, **16**, 3283.
37 J.-L. Roustan, N. Ansari, Y. Le Page and J.-P. Charland, *Can. J. Chem.*, 1991, **70**, 1650.
38 C. A. McAuliffe, in *Comprehensive Coordination Chemistry*, eds. G. Wilkinson, R. D. Gillard and J. A. McCleverty, Pergamon, Oxford, 1987, vol. 2, ch. 14, p. 1030.
39 R. L. Martin and D. Taylor, *Inorg. Chem.*, 1976, **15**, 2970.
40 J. H. Enemark and R. D. Feltham, *Top. Stereochem.*, 1981, **12**, 155.
41 F. H. Allen, O. Kennard and R. Taylor, *Acc. Chem. Res.*, 1983, **16**, 146; F. H. Allen, Davies, J. J. Galloy, O. Johnson, O. Kennard, C. F. Macrae, E. M. Mitchell, G. F. Mitchell, J. M. Smith and D. G. Watson, *J. Chem. Inf. Comput. Sci.*, 1987, **31**, 187.
42 B. F. G. Johnson, B. L. Haymore and J. R. Dilworth, in *Comprehensive Coordination Chemistry*, eds. G. Wilkinson, R. D. Gillard and J. A. McCleverty, Pergamon, Oxford, 1987, vol. 2, ch. 13.3, p. 99.
43 D. M. P. Mingos and D. J. Sherman, *Adv. Inorg. Chem.*, 1989, **34**, 293.
44 J. H. Enemark and R. D. Feltham, *Coord. Chem. Rev.*, 1974, **13**, 339.
45 D. Ballivet-Tkatchenko, C. Esselin, and J. Goulon, *J. Phys. Colloq.*, 1986, **47**, C8; M. F. Ruiz-Lopez, M. Loos, J. Goulon, C. R. Natoli and D. Ballivet-Tkatchenko, *Physica B*, 1989, **158**, 200.
46 K. S. Chong, S. J. Rettig, A. Storr and J. Trotter, *Can. J. Chem.*, 1979, **57**, 3113.
47 B. Haymore and R. D. Feltham, *Inorg. Synth.*, 1973, **14**, 82.
48 R. B. King, *Organomet. Synth.*, 1965, **1**, 167.
49 J. C. Smart and B. L. Pinsky, *J. Am. Chem. Soc.*, 1980, **102**, 1009.
50 R. B. King, *Organomet. Synth.*, 1965, **1**, 70.
51 D. W. McBride, S. L. Stafford and F. G. A. Stone, *Inorg. Chem.*, 1962, **1**, 386.
52 G. M. Sheldrick, SHELXTL-PLUS, Rev. 4.1, Göttingen, Germany, 1990.
53 *International Tables for X-Ray Crystallography*, Kynoch Press, Birmingham, vol. 4, 1974.

Received 21*st February* 1996; *Paper* 6/01265E